Pressure-induced phase transitions of the $LiAlD_4$ system

M. P. Pitt,* D. Blanchard, and B. C. Hauback
Physics Department, Institute for Energy Technology, P.O. Box 40 Kjeller, N-2027 Norway

H. Fjellvåg
Centre for Materials Science and Nanotechnology, Department of Chemistry, University of Oslo, P.O. Box 1126 Blindern, N-0318 Norway

W. G. Marshall
ISIS Facility, Rutherford Appleton Laboratory, Chilton, Didcot OX11 0QX, United Kingdom
(Received 28 June 2005; revised manuscript received 17 August 2005; published 9 December 2005)

Compression of the $LiAlD_4$ system has been studied using *in situ* time-of-flight neutron diffraction up to 7.15 GPa and 60 °C. At ambient temperature (T_a), the structure remains as monoclinic α-$LiAlD_4$ up to 7.05 GPa, displaying a 26.9% reduction in unit cell volume to 200.9 Å^3, yielding a 28.7% increase in volumetric efficiency to 136.5 kg D_2/m^3. Decompression to a small 3 ton load at T_a and holding for 24 hours did not induce any phase transformation, and the starting 0 GPa α-$LiAlD_4$ structure was eventually recovered. Heating from T_a to 60 °C while under compression to 7.15 GPa produces new and intense reflections in the diffraction pattern, while also retaining α-$LiAlD_4$ reflections, indicating a two-phase α/β-$LiAlD_4$ mixture. The β-$LiAlD_4$ structure indexed from this data is in the monoclinic space group $I2/b$, with unit cell dimensions $a=4.099(3)$ Å, $b=4.321(4)$ Å, $c=10.006(7)$ Å, $\gamma=88.43(2)°$, yielding a volumetric efficiency of 151.2 kg D_2/m^3. The atomic arrangement in $I2/b$ is identical to that in the theoretically predicted $I4_1/a$ super group, with isolated symmetric AlD_4 tetrahedra displaying Al—D distances of 1.545(2) Å. Once again, decompression and cooling recovers the ambient α-$LiAlD_4$ structure.

DOI: 10.1103/PhysRevB.72.214113 PACS number(s): 61.12.−q

I. INTRODUCTION

Hydrogen storage materials have received considerable attention recently, with the international community specifying mobile transportation capacities of greater than 5 and 6 wt. % hydrogen.[1,2] Focus has thus shifted away from heavy metallic and intermetallic alloys, and turned to complex hydrides formed from the lightest of elements, such as the aluminohydrides (alanates), borohydrides, and amides/imides. Alkali-earth alanates such as $LiAlH_4$ and $NaAlH_4$ hold a theoretical 10.6 and 7.5 wt. % respectively. Recent improvements in kinetics and reversible capacity have been achieved with transition metal catalysis,[3] yielding a stable and reversible 4–5 wt. % cycling capacity up to 100 cycles for the $NaAlH_4$ system in the 120 °C–160 °C temperature range.[4–7] The $LiAlH_4$ system is in contrast quite unstable,[8] and reversibility has not yet been demonstrated.

Alanates typically display moderate volumetric hydrogen storage capacity, up to 100 kg H_2/m^3. Recent theoretical studies by our group have shown that significant increases in volumetric efficiency up to 17% can be achieved for a range of alanates, utilizing high-pressure phase transitions.[9–12] Among the candidates, the $LiAlH_4$ system shows the most promise. The ambient α-$LiAlH_4$ $P2_1/c$ structure[13] is predicted to transform at a modest 2.6 GPa to β-$LiAlH_4$ $I4_1/a$ (α-$NaAlH_4$ structure), with an attendant 17% reduction in unit cell volume. For the $NaAlH_4$ system, only a moderate 4% reduction is predicted at 6.4 GPa, modifying α-$NaAlH_4$ $I4_1/a$ to β-$NaAlH_4$ $Cmc2_1$.

A review of reported experimental high-pressure work for the $LiAlH_4$ system shows only five significant studies that are now relatively old, and that were conducted using *ex situ* methods.[14–18] These studies report temperature dependent β- and γ-$LiAlH_4$ crystal structures, electrical resistivity of $LiAlH_4$ with pressure, β-Li_3AlH_6 crystal structure, and two different pressure-temperature phase diagrams, respectively. However, the analysis is typically from old medium resolution laboratory source x-ray diffractometers that cannot reveal H positions, no diffraction patterns are shown, and only tables of the most intense d spacings are provided. In this regard, the crystal structures reported must be considered as preliminary results only. Based on improved diffraction measurements, it is proposed from the phase diagram developed in the latest work[18] that the γ-$LiAlH_4$ crystal structure does not exist, and that beyond 523 K, β-$LiAlH_4$ decomposes to either α- or β-Li_3AlH_6 depending on the temperature range.

Much more recent experimental tests of the predicted α- to β-$LiAlH_4$ transition have been completed by Talyzin *et al.*,[19] utilizing Raman spectroscopy. Spectra collected under pressure at ambient temperature display a splitting from doublet to triplet, at pressures very close to the predicted transition pressure of 2.6 GPa. The splitting occurs reversibly in pressure, and extends over ca. 1 GPa in range, indicating possible multiple phase coexistence. Assuming that the phase transformation is eventually completed and the sample is single phase, such a triplet structure implies a distortion of the symmetry of the AlH_4 tetrahedra. Such phase coexistence and reversibility has also been observed by Bulychev *et al.*,[14] using a combination of *ex situ* x-ray diffraction and Raman spectroscopy. The Raman spectra collected in this experiment extend to 2000 cm^{-1}, however no triplet is observed. Further, the diffraction data are clear that the

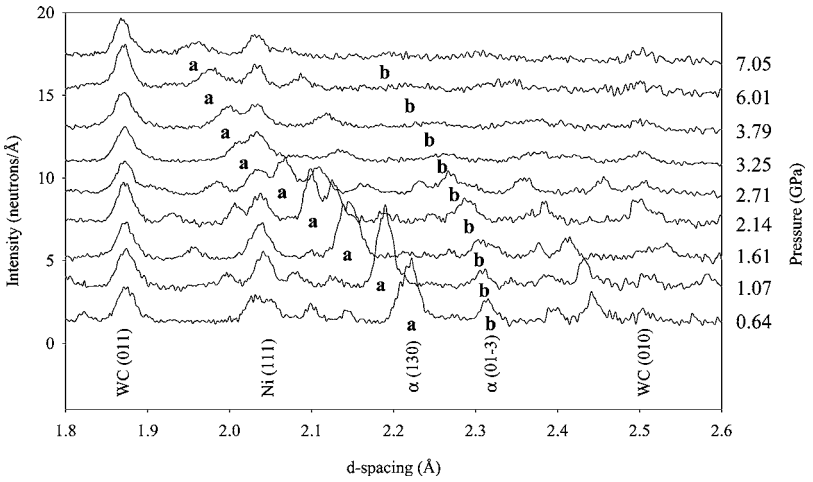

FIG. 1. Ambient temperature data sequence of α-$LiAlD_4$ up to 7.05 GPa over the *d*-spacing range 1.80–2.60 Å. Sample pressure is indicated on the right. Significant differences can be observed in individual reflection *d*-spacing shifts, such as *a* and *b*, the α (130) and α (01-3) reflections, respectively. Significant loss of diffracted intensity is observed from 3.25 GPa onward.

α-$LiAlH_4$ $P2_1/c$ structure does not transform at ambient temperature, even under 7 GPa. Only with temperatures greater than ambient can a phase transformation take place, and in this regard, the Raman measurements of Talyzin *et al.*[19] display features of ambient temperature, pressure induced distortion of the α-$LiAlH_4$ $P2_1/c$ structure.

To resolve the question of the possible distortion of the AlH_4 tetrahedra, and to provide a stronger crystallographic perspective, we have studied the $LiAlD_4$ deuteride system under varying pressure and temperature, up to 7.15 GPa and 60 °C, using *in situ* time-of-flight (TOF) neutron diffraction.

II. EXPERIMENTAL PROCEDURE

$LiAlD_4$ (quoted $\geqslant$98% purity) was purchased from Sigma-Aldrich. High-resolution diffraction patterns collected on HRPD ISIS indicate minimal impurity levels, and the sample contains only 0.03 wt. % LiCl. Powders were at all times handled in inert He atmosphere.

Neutron powder diffraction data were collected using the high flux, medium-resolution ($\delta d/d = 0.85\%$) time-of-flight diffractometer, HiPr, on the PEARL beamline at the ISIS Neutron Facility, Rutherford Appleton Laboratory. PEARL/HiPr is optimized for measurements in $2\theta = 90°$ scattering geometry using the Paris Edinburgh cell, utilizing nine detector modules each consisting of 120 Li^6-doped/ZnS scintillator elements situated over the range $2\theta = 83° - 97°$.[20] The incident beam is highly collimated, and illuminates a ca. 88 mm^3 initial sample volume inside the pressure cell. The pressure cell is a V4b-type Paris Edinburgh cell using WC/Ni-binder anvils rated to ca. 10 GPa, and uses a null matrix Ti—Zr alloy capsule gasket to protect the sample from atmosphere.[21,22] The cell can be safely operated to 60 °C using band heaters. Small amounts of either NaCl or Pb are added to the sample as pressure calibrants. Fluorinert [grades FC-75 (first experiment) and 1:1 by volume FC-87/FC-84 (second experiment)] was used as a pressure-transmitting medium. The standard MeOD/EtOD mixture was avoided to prevent reduction of the $LiAlD_4$ with water or alcohol. Our first experiment was conducted at ambient temperature only. The second follow up experiment repeated our first ambient measurements more carefully, but also importantly included hotter measurements at 60 °C. During our second series of ambient measurements, our Pb pressure calibration marker fell out of the beam at very low load, but fortunately we have an accurate NaCl pressure scale from our first measurements. The Pb marker for our 60 °C measurements remained in the beam at all times. This explains why no reflections from Pb are present in our second series of ambient temperature data presented below. The *d*-spacing focussed and attenuation-corrected diffraction patterns were analyzed using GSAS (Ref. 23) and RIETICA.[24] Diffraction line profiles were fitted using the double-exponential pseudo-Voigt, with instrumental parameters determined from Si and CeO_2 standards normalized to a vanadium spectrum. Backgrounds were fitted with type I or II Chebyshev polynomials. Both free and soft constrained refinements of interatomic distances were performed for all crystal structure determinations of hydride phases. Our soft constraints model in GSAS specified minimum interatomic separations as Al—D $\geqslant$ 1.55 Å, Li—D $\geqslant$ 1.70 Å, Al—Al $\geqslant$ 2.70 Å, Li—Li $\geqslant$ 2.70 Å, Li—Al $\geqslant$ 2.40 Å, and D—D $\geqslant$ 2.10 Å. For the $LiAlD_4$ system, data was collected at both ambient temperature and 60 °C, to a maximum pressure of 7.15 GPa.

III. RESULTS AND DISCUSSION

A. Ambient temperature pressure-dependent distortion of α-$LiAlD_4$

The first part of the experiment aimed to study the compression of the α-$LiAlD_4$ $P2_1/c$ unit cell structure at ambient temperature only. Diffraction patterns collected at ambient temperature up to 7.05 GPa are shown in Fig. 1, showing the most interesting variation of intensities over the *d*-spacing range 1.80–2.60 Å. With a low monoclinic starting symmetry, and significant neutron absorption due to use of natural Li [σ_{abs}(Li) = 70.5 barn] collected at medium $\delta d/d$ resolution, it becomes difficult to follow the compression of individual reflections, and it is clear from initial refinements of the data that some reflections such as (130) are significantly shifted, while others such as (01-3) are initially only moderately shifted (reflections are labelled as *a* and *b*, respectively, in Fig. 1), and that considerable reductions in diffracted

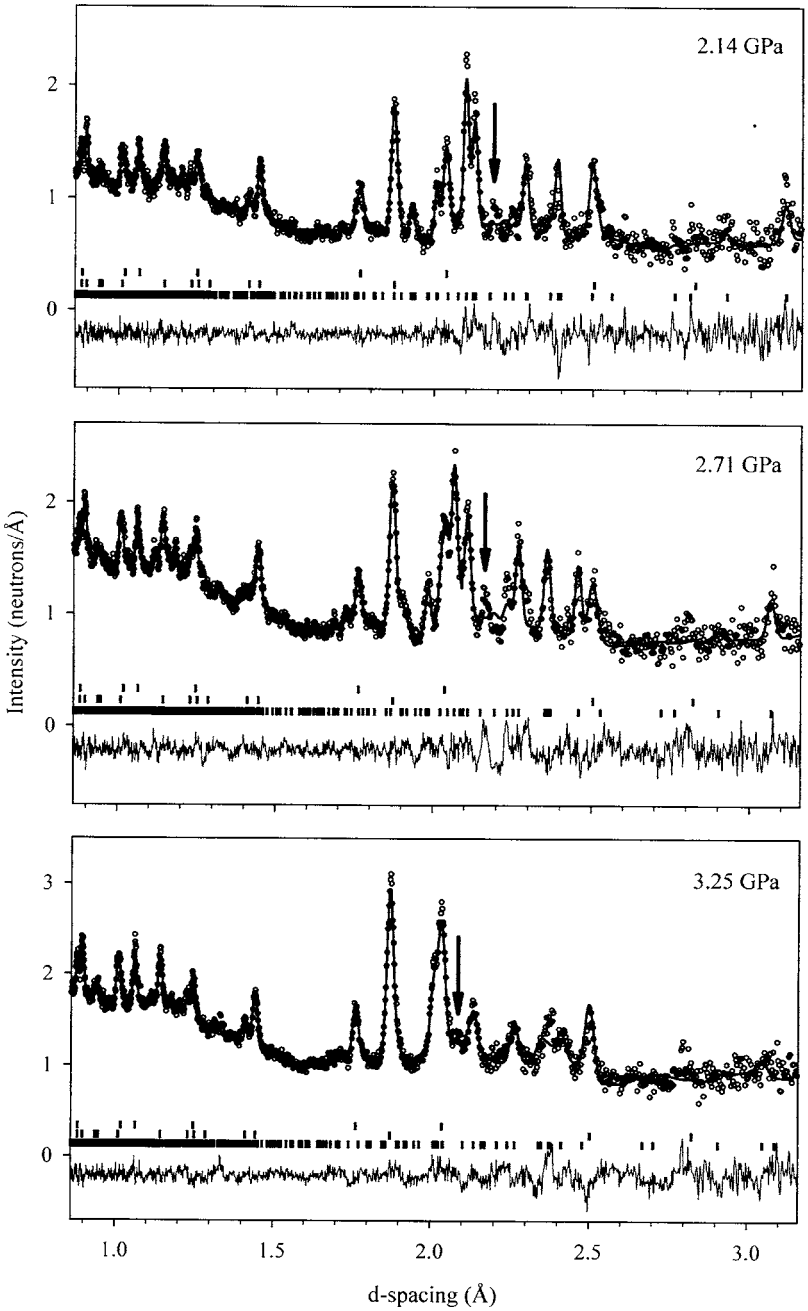

FIG. 2. Rietveld refined diffraction patterns of the ambient temperature data series, below, close to, and above the theoretically predicted transition pressure of 2.6 GPa. In each figure, the data is represented by the points (○), and the upper solid line shows the model calculation. The upper set of reflection markers is from the Ni binder used in the anvils, the middle set from the WC anvils, and the lower set corresponds to the α-$LiAlH_4$ phase. The difference profile (I_{obs}-I_{calc}) showing the quality of fit is below the reflection markers. The unindexed reflection discussed in Sec. III A is indicated by arrows in each diagram.

sample intensity are occurring by high pressures. Thus, the structural refinement strategy necessarily started with patterns at low pressures, where indexing of the unit cell was clear from numerous and intense peaks. Figure 2 compares Rietveld refinements before and after the predicted transition pressure.

It can be observed in Fig. 2 that although almost all of the intensity in the diffraction pattern can be accounted for by the α-$LiAlD_4$ structure, one peak at ~2.2 Å remains unindexed by the α-$LiAlD_4$ $P2_1/c$ unit cell. This peak appears at low pressure, and continues to grow in intensity and also compress as a function of pressure. There exist three possibilities to explain the presence of this new peak. (i) The sample has partially decomposed under pressure, forming α-Li_3AlD_6, and free Al. (ii) The sample has reacted with the pressure-transmitting medium, fluoroinert (C_mF_n), suggesting the formation of a fluoride or carbide, or (iii) the monoclinic α-$LiAlD_4$ $P2_1/c$ unit cell has suffered a lower symmetry distortion. All cases have been thoroughly tested. Case (i) can be ruled out on the basis that any free Al present placed at the unindexed position is clearly not at the correct d spacing for the applied pressure. Further, the phase diagram developed by Konovalov *et al.*[18] indicates decomposition under pressure does not occur until beyond 523 K. Case (ii) presents the widest range of possibilities, and indexing has been tested against the candidates LiF, AlF_3, Li_2C_2, and also LiD. Li_2O has also been included as the commonly formed oxide for $LiAlD(H)_4$. The behavior of the fluorides[25–27] and the deuteride[28] under pressure are known and they can be ruled out, however a literature search reveals no information about the carbides under pressure. However, at very low pressure, the Li_2C_2 cell is clearly too far away in

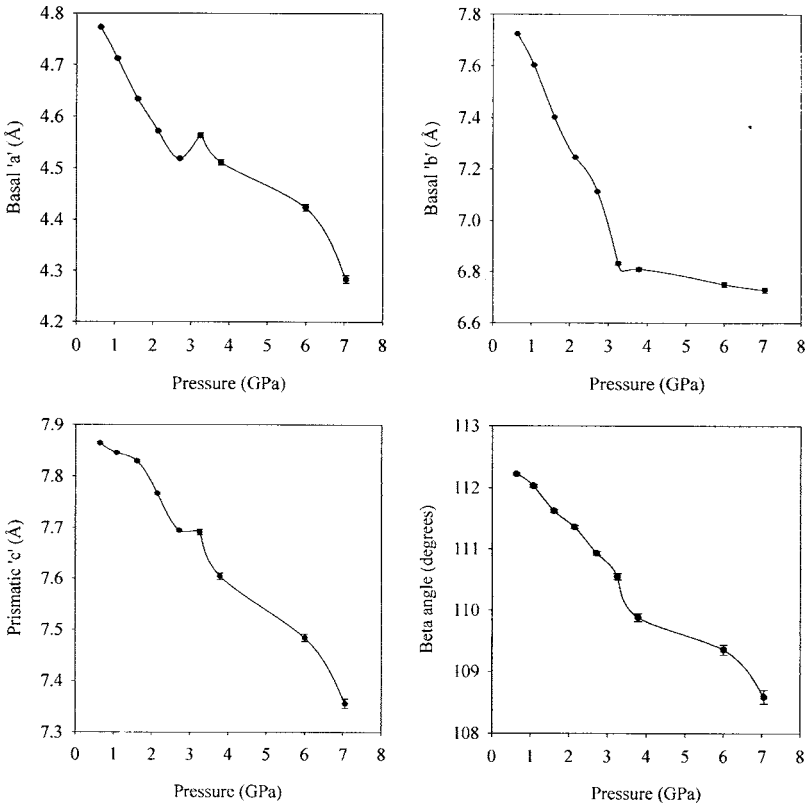

FIG. 3. The variation of basal and prismatic lattice parameters, and unit-cell angle of the α-$LiAlD_4$ phase across the entire pressure range. Prominent kinks can be observed in the *a* and *c* axis, very close to the predicted transition pressure of 2.6 GPa. Extrapolating the observed behavior beyond 7.05 GPa suggests the unit cell can be compressed even further below 200 $Å^3$.

d spacing.[29] Similarly, the Li_2O cell is also too far away in *d* spacing.[30] The most important observation regarding both cases (i) and (ii) is that this peak is present in the data collected after decompression, when only pure α-$LiAlD_4$ is present, indicating that no decomposition and subsequent formation of α-Li_3AlD_6 took place. This suggests that a side reaction has occurred that has reduced a small percentage of the sample. This idea is further supported in our unpublished data on the $NaAlD_4$ system under pressure, which shows the development of a similar peak, albeit at slightly larger *d* spacings, logically suggesting the formation of Li_z-X_y and Na_z-X_y type phases. As free Al is not observed, it would necessarily be amorphous or strongly nanocrystalline. Assuming that not all the Al is amorphously dispersed, the remaining possibility is Li_3AlF_6, and upon further testing, for both the $NaAlD_4$ and $LiAlD_4$ systems, adequate fits can be obtained to the unindexed peak with the hexafluoride structures. This suggests that D and F has exchanged between the sample and the fluoroinert. It is possible to confirm this exchange by dry compression tests with no fluoroinert present, however, the interpretation of this dry data may be completely compromised due to the expected nonhydrostatic pressure induced line broadening that will occur in the complete absence of a pressure transmitting medium. Although we can offer no further experimental evidence of a D/F exchange, such chemistry is common in AlF_3 catalysis of fluorohydrocarbon transformations that can cause C—F bond rearrangements.[31] Case (iii) has been ruled out with indexing tests in Dicvol,[32] and no other monoclinic or lower symmetry triclinic solutions can be found that do not remove clearly intense *d* spacings to produce an alternative unit cell. However, the indexing of medium resolution data can be problematic,[33] and further intensity independent Le Bail tests[34] were conducted to produce possible lower symmetry triclinic cells. These cells were then used in two-phase tests of possible atomic arrangements using the new TOF version of FOX.[35] No adequate solutions could be found below $\chi^2=30$ after $>10^9$ iterations. For future investigations, higher resolution data for improved indexing tests is desirable to unambiguously rule out any contribution from the extra peak. With this knowledge that the extra peak is likely not part of the $LiAlD_4$ structure, it can be excluded or modelled as Li_3AlF_6 within the Rietveld refinements, and all diffraction patterns up to 7.05 GPa are then excellently indexed with the α-$LiAlD_4$ $P2_1/c$ structure, with χ^2 and R_{wp} falling in the range 1.274–2.045 and 0.045–0.058, respectively.

The variation of unit cell dimensions of the α-$LiAlD_4$ $P2_1/c$ structure with pressure are shown in Fig. 3. A prominent kink occurs in the variation of all cell dimensions at ca. 3 GPa, very close to the theoretically predicted transition pressure, and it is clear that the basal *b* axis is close to its compression limit by this pressure. Although the basal *b* axis will yield little further compression, extrapolation of all other unit cell metrics indicates that the unit cell volume can be decreased further below 200 $Å^3$ upon application of higher pressures. Even with reduced intensities beyond 3 GPa, the crystal structure clearly remains α-$LiAlD_4$. In this sense, we regard the peculiar compression behavior of the cell through the predicted transition region as a struggle to transform to β-$LiAlD_4$ at ambient temperature. This is also suggested by the massive reduction in unit cell volume, from ca. 270 $Å^3$ to ca. 200 $Å^3$, yielding an impressive 26.9% reduction. Of this 26.9% reduction, ca. 20% is achieved by 3 GPa, yielding a ca. 220 $Å^3$ unit cell which falls extremely close to the pre-

TABLE I. Ambient α-$LiAlD_4$ crystal structures, with atoms at positions determined by the soft constraints model. (a) $T=T_a\approx 20$ °C, $P=2.71$ GPa; space group $P2_1/c$; $a=4.518(1)$ Å, $b=7.115(2)$ Å, $c=7.694(2)$ Å, $\beta=110.93(3)°$; $R_{wp}=0.061$, $\chi^2=2.045$. (b) $T=T_a\approx 20$ °C, $P=3.25$ GPa; space group $P2_1/c$; $a=4.563(3)$ Å, $b=6.833(4)$ Å, $c=7.692(5)$ Å, $\beta=110.57(7)°$; $R_{wp}=0.055$, $\chi^2=1.961$.

Site	Atom	x	y	z	B_{iso}[a,b]	Occupancy
			(a)			
4*e*	Li	0.514(8)	0.464(5)	0.822(4)	1.9(3)	1.0000
4*e*	Al	0.106(3)	0.209(2)	0.921(2)	1.9(4)	1.0000
4*e*	D1	0.228(5)	0.072(2)	0.794(2)	2.8(1)	1.0000
4*e*	D2	0.289(5)	0.410(2)	0.952(2)	2.8(1)	1.0000
4*e*	D3	0.195(4)	0.120(2)	0.118(2)	2.8(1)	1.0000
4*e*	D4	0.708(4)	0.238(3)	0.819(3)	2.8(1)	1.0000
			(b)			
4*e*	Li	0.535(9)	0.475(7)	0.817(5)	1.9(3)	1.0000
4*e*	Al	0.128(5)	0.197(4)	0.945(3)	1.9(4)	1.0000
4*e*	D1	0.218(8)	0.058(5)	0.805(4)	2.8(1)	1.0000
4*e*	D2	0.332(7)	0.392(5)	0.979(4)	2.8(1)	1.0000
4*e*	D3	0.202(7)	0.089(5)	0.139(4)	2.8(1)	1.0000
4*e*	D4	0.754(8)	0.252(5)	0.853(5)	2.8(1)	1.0000

[a]Isotropic thermal parameters have been fixed at magnitudes determined from low pressure refinements, to avoid the artefactual negative magnitudes that can occur due to the strong loss of diffracted sample intensity at higher pressures.

[b]Deuterium thermal parameters have been refined at a common magnitude.

dicted equilibrium β-$LiAlH_4$ unit cell volume[10] of 228.6 Å^3. It is clear then that pressure alone is not enough to produce the β-$LiAlH_4$ structure, and temperature is required to produce the activation energies needed to drive the bond breaking required for the α to β phase transition, as discussed further in Sec. III B. This interpretation is consistent with the original phase diagram developed by Bulychev *et al.*,[14] which indicates the structure remains α-$LiAlH_4$ at ambient temperature.

With the significant reduction in intensity that occurs after 3 GPa, the free refinement of the $P2_1/c$ unit cell structure becomes unstable, and it becomes necessary to use soft interatomic distance and tetrahedral angle constraints to avoid unphysical short separations. Even with the soft constraints model in GSAS, it is clear that distortion of the AlD_4 tetrahedra is always possible, and variation in bond lengths and angles can be consistently observed. Observation of intensity misfits in our data reveals that when the D positions are freely refined from their soft constrained positions, subsequent distortion of the AlD_4 tetrahedra can recover significant misfits in some reflections, consistent with the interpretation of Raman data by Talyzin *et al.*[19] Residual intensity misfit in the difference profile is observable in all patterns in Fig. 2, and has deliberately been left to emphasize that the soft constraints model must eventually be switched off, and D atoms allowed to refine to free positions to recover intensity misfits. This must be done carefully to avoid unphysical short interatomic separations.

It should also be noted that Talyzin *et al.*[19] used a 4:1 ethanol:methanol mixture as the pressure transmitting medium for their experiments, and it is possible that the $LiAlH_4$ has reacted and produced at least LiOH.[36] The high chemical reactivity of alanates with oxygen, water, and alcohols is problematic, and side reactions with the pressure-transmitting medium appear unavoidable. The possible presence of multiple phases in the sample thus makes interpretation of the Raman data complex. Clearly neutron diffraction data are more desirable to directly measure AlD_4 tetrahedral properties.

Table I presents our final structural parameters for the α-$LiAlD_4$ structure before and after the 3 GPa kink region. The metal and D atoms are at positions determined within the flexibility of the soft constraints model in GSAS, in this case, with tetrahedral angles determined about the ideal angle 109.47°, constrained by the esd 2.0, and Al—D distances constrained about 1.60 Å with esd 0.1 (The estimated standard deviation, esd, is defined in the soft constraints model in GSAS such that a very low esd will induce a large increase in the global χ^2, which will force the interatomic separation very close or equal to the specified value. A softer constraint with a high esd will allow the interatomic separation to relax about the specified separation. In that sense, the esd of 2.0 for Al—D—Al tetrahedral angle can be considered moderate, while the esd of 0.1 for Al—D is considered hard.) With this methodology, bond lengths and tetrahedral angles can be observed to fall in the range 1.559(2)–1.725(2) Å and 105.9(9)–111.4(2)°, respectively over the entire pressure range. Figure 4 shows the variation of Al—D distances and AlD_4 tetrahedral angles over the entire pressure range. Our results are consistent with the doublet to triplet splitting in the Raman spectra presented by Talyzin *et al.*[19] The largest deviations from the ideal Al—D

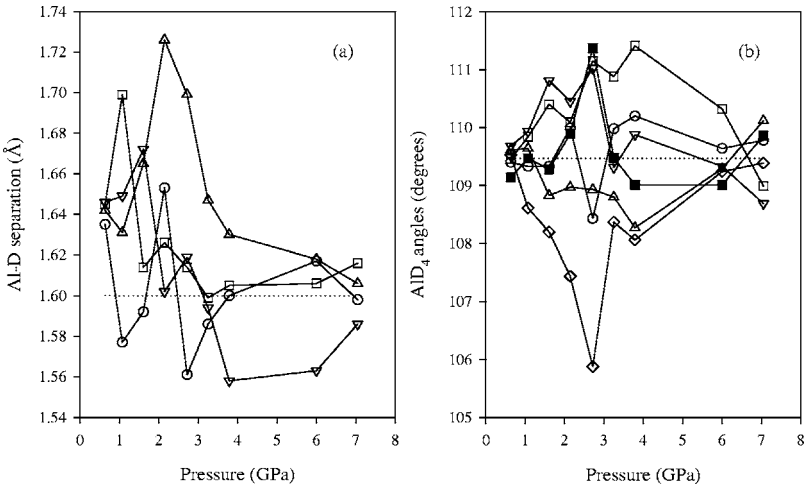

FIG. 4. Properties of the AlD_4 tetrahedra under pressure at ambient temperature. (a) Al—D interatomic separation. Points labeled as (□), (△), (○), and (▽) refer to Al-D1, Al-D2, Al-D3, and Al-D4 separations, respectively. (b) AlD_4 tetrahedral angles. Points labeled as (▽), (○), (△), (◇), (■), and (□) refer to D1-Al-D2, D1-Al-D3, D1-Al-D4, D2-Al-D3, D2-Al-D4, and D3-Al-D4 separations, respectively. The scatter in distances and angles agrees well with the Raman spectra reported by Talyzin *et al.* (Ref. 19), where splitting is observed very close to the predicted transition pressure of 2.6 GPa, indicating distortion of the AlD_4 tetrahedra. The convergence of distances and angles to ideal values at higher pressures is artefactual due to significant loss of diffracted sample intensity.

distance of 1.60 Å and tetrahedral angle of 109.47° occur in the 2–3 GPa region, exactly where the theoretically predicted phase transition should occur. After 3.79 GPa, both distances and angles can be seen to approach ideal magnitudes. This is artefactual, and occurs as a result of the significant decrease in diffracted intensity in the 6.01 and 7.05 GPa data. Physically, as observed by the splitting that remains in the Raman spectra of Talyzin *et al.* up to 6 GPa,[19] the AlD_4 tetrahedra can be considered to remain distorted at higher pressures.

The close agreement of the transition pressure between theory[10] (H based calculation), and experimental measurements of H based[19] and D based (this work) samples also suggests that there is little or no pressure induced isotope effect in the $LiAlH(D)_4$ system, within the pressure range studied to date.

B. Two-phase α/β-$LiAlD_4$ mixture at 60 °C and 7.15 GPa

The second part of our experiment aimed to use the knowledge gained from our ambient temperature measurements, and to use temperature to attempt to produce the β-$LiAlD_4$ phase. After first placing a new sample under ca. 1 GPa at ambient temperature to ensure no loss of fluoroinert with temperature, both temperature and pressure were slowly increased incrementally until 7.15 GPa and 60 °C were reached. Figure 5 shows the diffraction pattern obtained at 7.15 GPa and 60 °C, with the final calculated and difference profiles. New and intense peaks can be observed in the diffraction pattern (indicated as arrows in Fig. 5) amidst existing α-$LiAlD_4$ peaks, suggesting that a two-phase mixture has formed, again consistent with the original phase diagram of Bulychev *et al.*,[14] that indicates a two-phase α/β mixture remains until past 250 °C when pure β-$LiAlH_4$ is obtained.

Indexing the most intense reflection of the new phase on the side of the (101) WC anvil reflection with the theoretical tetragonal β-$LiAlH_4$ structure yields unit cell dimensions of $a=4.355(3)$ Å and $c=10.017(2)$ Å. Multiple-phase α/β-$I4_1/a$ test refinements immediately showed several unstable features in both structures. Throughout the course of all space groups tested for the β-structure, the monoclinic α-structure consistently displayed problems with intensity over-fit in the longer d-spacing region beyond 2.6 Å. The β-structure in $I4_1/a$ does not index any reflections in the range 2.65–3.99 Å, and it is clear that the monoclinic α-phase reflections in this range are reduced to negligible intensities. The only feature in the α-structure that allowed for a reduction in intensities in this range was distortion of the AlD_4 tetrahedra, and the tetrahedral angle constraints model used in GSAS must be slackened. Physically it is expected that the AlD_4 tetrahedra in the α-structure will become disordered in the transition to the β-structure, also explaining the loss of longer d-spacing intensity. Structural rearrangement is a necessity, and bond breaking is expected in the first coordination sphere. The final refined structure for the α-phase allows a protrusion of the Al atom through the

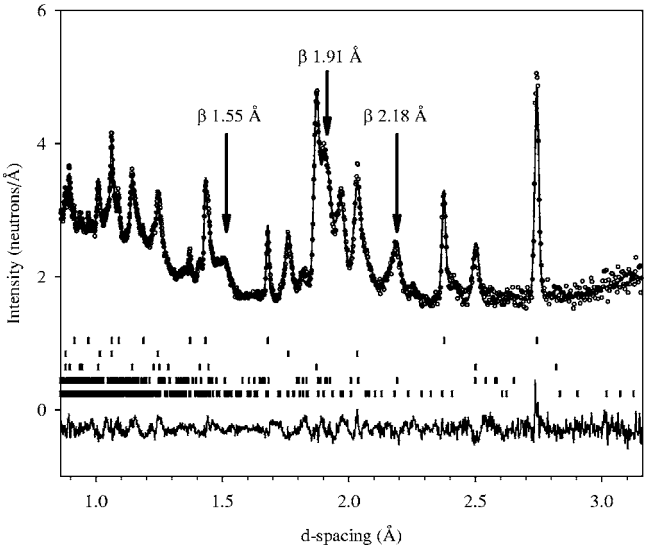

FIG. 5. Rietveld refined diffraction pattern of a two-phase α/β mixture at 60 °C and 7.15 GPa. Arrows indicate new and intense peaks from the β-phase at d spacings of 1.55, 1.91, and 2.18 Å. Data is represented by the points (○), and the upper solid line shows the model calculation. The sequence of reflection markers from top to bottom is Pb, Ni, WC, β-$LiAlD_4$, and α-$LiAlD_4$. The difference profile (I_{obs}-I_{calc}) showing the quality of fit is below the reflection markers. Most residual misfit in the difference profile comes from the high symmetry phases, Ni, WC, and Pb.

tetrahedral face defined by D atoms D2-D3-D4, with tetrahedral angles falling in the range 94.8(1)°–129.7(2)°, while maintaining valid Al—D distances in the range 1.545(7)–1.622(2) Å. Although we can offer no further experimental evidence as to the physical validity of such a protrusion, it is the only feature that reproduces about zero intensity through the 2.65–3.99 Å region. All interatomic separations fall in normal ranges, except for one Li—Al distance observed at 2.616(2) Å. Such shortened intermetallic separations are not unexpected under pressure.

Refinement of the β-structure in space group $I4_1/a$ showed several unstable features. Initially, free refinement of Al and D positions leads to short Al—D separations of ca. 1.33 Å. In general, strongly background correlated structural instability in $I4_1/a$ can be observed as intensity under-fits at the new β peak positions at 1.50 and 1.91 Å, and as severe over-fit at the longer d-spacing 3.99 Å, both of which free refinement of the background will attempt to compensate for. Positional misfit can also be observed at the (121) position. If Al—D distances in the β-structure are constrained to 1.55 Å, severe intensity under-fit will occur on (121), while removing the longer d-spacing misfit at 3.99 Å. It is clear then that part of the new peak intensity at both 1.55 and 1.91 Å must be produced from the monoclinic α-structure. Refining the α-structure further can lead to considerable improvements of the fit, however, instability remains in both structures. In compensating part of the intensity at 1.91 Å, residual intensity over-fits will remain for the α-structure in the intensity poor 2.65–3.99 Å region. Correlated with the instabilities in the α-structure are instabilities in the β-tetrahedra. Constraining β Al—D distances to 1.55 Å will lead to D—D separations shorter than 2.10 Å, in violation of the Switendick criterion.[37] Although shortened D—D separations are feasible under pressure, in this case, the feature is born from correlated instability, rather than any physical basis. Forcing a minimum 2.10 Å separation on two edges of the tetrahedra leads to strong deviations from the ideal tetrahedral angle of 109.47°, with contracted and expanded angles of 85.1(2)° and 122.9(2)°, respectively.

The final multiphase α/β-$I4_1/a$ fit obtained can be deemed reasonable at a $\chi^2=4.701$ and $R_{wp}=0.041$, however it is clear that attempts to force a β-structure solution in $I4_1/a$ forces the α-structure to diverge considerably from its structural minimum. Perhaps the most crucial feature indicating lower symmetry than $I4_1/a$ is the positional misfit at 1.91 Å, and that (220) and (222) both fall too far below and above in d spacing from the new 1.55 Å peak to contribute any intensity. Even with residual background correlated intensities for both phases, it is still clear that the intensity contribution from the $I4_1/a$ model is reasonably close. Considering the positional misfit and the close intensities for $I4_1/a$, the next logical choice of symmetry descends the subgroup chain below $I4_1/a$ to preserve the atomic arrangement, but allow a distortion of the unit-cell geometry. The monoclinic subgroup $I2/b$ (nonstandard setting of $C2/c$) allows a monoclinic distortion of the unit cell, and splits the single D site in $I4_1/a$ across two positions.

Allowing monoclinic distortion in both unit cells can lead to considerable difficulties in indexing the correct unit cell of each phase. By necessity, the ambient temperature 7.05 GPa α-structure is used as a starting point for the α-structure, and the split D sites in the β-structure are started at positions from the ideal ambient structure. These two structures are then held constant, while the unit cell dimensions are refined. This proved to be an extremely effective and stable refinement strategy. It was immediately clear that the β unit cell is distorted from ideal tetragonal geometry, and the subsequent reflection splitting in monoclinic geometry removed all positional misfits, while preserving the atomic arrangement present in the $I4_1/a$ structure. Intensity background correlations were also removed from the α-structure, and an excellent fit was obtained through the intensity poor α region from 2.65–3.99 Å. After further refining both structures, an excellent fit could be obtained at a $\chi^2=3.113$ and $R_{wp}=0.033$. Final unit-cell dimensions are α-phase, $a=4.328(2)$ Å, $b=6.715(2)$ Å, $c=7.231(3)$ Å, $\beta=105.29(5)°$; β-phase, $a=4.099(3)$ Å, $b=4.321(4)$ Å, $c=10.006(7)$ Å, $\gamma=88.43(2)°$. The α unit cell is distorted slightly from its 7.05 GPa ambient temperature dimensions, showing a small compression of the prismatic axis and the β angle. It is also clear that the β-structure retains a distorted unit cell while it is present as part of a two-phase α/β mixture. The final β unit cell displays a strong orthorhombiclike compression of the a axis, and a moderate monocliniclike compression of the γ angle.

Although it has been proposed by Bulychev *et al.*,[14] Konavolav *et al.*[18] and Bastide *et al.*[17] that the Al atoms in the β-structure should coordinate as AlH_6 octahedra, their interpretation was based principally on Raman data, and medium resolution laboratory source x-ray diffraction data that cannot reveal information about H positions. Further, these early investigations did not have the benefit of guiding density functional based models. No feasible energetic basis for octahedrally coordinated Al can be found from the ground state β-phase calculations of Vajeeston *et al.*[10] It is also clear from our neutron diffraction data that excellent fits are obtained with tetrahedrally coordinated Al atoms. Further, there is no free compression of D—D distances in the AlD_4 tetrahedra in space group $I2/b$, as was observed for those in the $I4_1/a$ structure model. Al—D distances are all equal to 1.545(2) Å, with tetrahedral angles falling in the range 94.53(6)°–132.27(6)°. D—D separations in the tetrahedra do not need to be constrained, and range from 2.273(2)–2.829(1) Å. The shortest Li—D distance is 1.655(2) Å. No shortened intermetallic separations are observed. For the α-structure, the Al atoms were similarly allowed to protrude through one of the tetrahedral faces, while retaining viable Al—D distances. Again, the Li—Al separation proved to be the shortest separation observed, and was fixed at 2.40 Å. Atomic positions of both the α and β structures at 60 °C and 7.05 GPa are reported in Table II.

Phase proportion analysis shows that at 60 °C, the α:β molar proportion is ca. 1.7:1. A simple two-point linear extrapolation of the temperature-dependent molar proportion of the β-phase suggests that pure β can be obtained by ca. 140 °C, significantly lower than the 250 °C indicated by the *ex situ* quenched measurements of Bulychev *et al.*[14] We conclude that ground state 0 K calculations prove to be excellent indicators of predicted high-pressure structures. The experimentally determined unit-cell volume and atomic arrange-

TABLE II. Crystal structures of α-$LiAlD_4$ and β-$LiAlD_4$ at 60 °C and 7.15 GPa, with atoms at positions determined by the soft constraints model. (a) $T=60$ °C, $P=7.15$ GPa; α-$LiAlD_4$; space group $P2_1/c$; $a=4.328(2)$ Å, $b=6.715(2)$ Å, $c=7.231(3)$ Å, $\beta=105.29(5)°$; $R_{wp}=0.033$, $\chi^2=3.113$. (b) $T=60$ °C, $P=7.15$ GPa; β-$LiAlD_4$; space group $I2/b$; $a=4.099(3)$ Å, $b=4.321(2)$ Å, $c=10.006(3)$ Å, $\gamma=88.43(4)°$; $R_{wp}=0.033$, $\chi^2=3.113$.

Site	Atom	x	y	z	B_{iso}[a]	Occupancy
			(a)			
4*e*	Li	0.567(6)	0.435(3)	0.833(3)	1.9(3)	1.0000
4*e*	Al	0.022(6)	0.219(3)	0.932(5)	1.9(4)	1.0000
4*e*	D1	0.142(4)	0.083(3)	0.781(4)	2.8(1)	1.0000
4*e*	D2	0.253(4)	0.423(2)	0.958(3)	2.8(1)	1.0000
4*e*	D3	0.222(6)	0.126(4)	0.137(3)	2.8(1)	1.0000
4*e*	D4	0.690(5)	0.226(3)	0.981(3)	2.8(1)	1.0000
			(b)			
4*e*	Li	0.0000	0.2500	0.1250	1.9(3)	1.0000
4*e*	Al	0.0000	0.2500	0.6250	1.8(4)	1.0000
8*f*	D1	0.245(3)	0.441(4)	0.544(4)	2.9 (1)	1.0000
8*f*	D2	0.235(2)	0.467(5)	0.812(4)	2.9 (1)	1.0000

[a]Thermal parameters are fixed as described in Table I.

ment are extremely close to the theoretical prediction. Although speculative, it is possible that the monoclinic distortion of the β unit-cell symmetry is in this case a consequence of the two-phase nature of the system, deriving from the fact that the starting α-crystal seeds that β grows from are monoclinic. It is possible that when high enough temperature is reached to gain single-phase β-$LiAlH_4$ that the symmetry may increase from $I2/b$ to $I4_1/a$.

IV. CONCLUDING REMARKS

Thermodynamically, α-$LiAlH_4$ will clearly never be a practical H-storage material, as even the most optimistic evaluation of the formation enthalpy[8] shows that at kinetically optimal temperatures such as 140 °C, the first plateau pressure for Li_3AlH_6 formation from LiH and Al will occur at ca. 33 kbar. α-$LiAlH_4$ is simply too unstable. β-$LiAlH_4$ is only weakly separated in energy in the order of several meV/f.u. relative to α-$LiAlH_4$,[10] and a similar weak separation is also calculated for the α and β forms of Li_3AlH_6.[12] Thus, even if near ambient metastability could be achieved for β-$LiAlH_4$, due to the very weak separation of formation enthalpies between α and β forms, the β-phase is still an impractical material for hydrogen storage, with the first plateau pressure in the manometric phase diagram expected in the order of tens of kbar.

From the original work of Bulychev *et al.*,[14] β-$LiAlH_4$ quenched to ambient pressure and temperature inside 5 minutes was metastable long enough for diffraction measurements. However, the application of temperature quickly recovered the α-$LiAlH_4$ structure. The slower release of pressure and temperature in our neutron diffraction experiments recovered the α-$LiAlD_4$ structure immediately, and no metastability could be observed. In general, stabilizing high-pressure alanate phases at near ambient pressure may be problematic, particularly for hydrogen cycling tests at elevated temperature. Ground state calculations may prove useful in future experiments, to investigate features such as partial atom substitution that may assist in the lowering of hydrostatic transition pressures and enhanced ambient metastability of $MAlH_4$ and MBH_4 (M=Li, Na, K) high-pressure complex hydride phases.

A more promising use for the $LiAlH_4$ system is in the destabilization of higher wt. % and more stable hydrides such as $LiBH_4$, which holds a theoretical 18.5 wt. % hydrogen. The mixing of $LiBH_4$ with the less stable MgH_2 has recently demonstrated an 8–10 wt. % reversible system at ca. 350 °C and 10 bar,[38] an immense improvement on the 690 °C and 200 bar required to reabsorb hydrogen into SiO_2 catalyzed $LiBH_4$.[39] An appropriately catalyzed mixture of volumetrically efficient ambient metastabilized β-$LiAlH_4$ and high wt. % α-$LiBH_4$ holds much promise and a new investigative pathway for finding thermodynamically practical hydrogen storage materials.

ACKNOWLEDGMENTS

The authors would like to acknowledge the EC for partial financial support through the European Project HYSTORY, Contract No. ENK6-CT-2002-00600. The authors also acknowledge the skillful assistance of the ISIS user support team.

*Corresponding author. Electronic address: mark.pitt@ife.no

[1] Task 17: Solid and Liquid State Hydrogen Storage Materials, edited by G. Sandrock (http://hydpark.ca.sandia.gov/ieaframe.html).
[2] FY 2004 Progress Report for Hydrogen, Fuel Cells, and Infrastructure Technologies Program, US Department of Energy, 2004. (http://www.eere.energy.gov/hydrogenandfuelcells/annual_report04.html).
[3] B. Bogdonavic and M. Schwickardi, J. Alloys Compd. **253/254**, 1 (1997).
[4] G. Sandrock, K. Gross, and G. Thomas, J. Alloys Compd. **339**, 299 (2002).
[5] M. Fichtner, O. Fuhr, O. Kircher, and J. Rothe, Nanotechnology **14**, 778 (2003).
[6] S. S. Srinivasan, H. W. Brinks, B. C. Hauback, D. Sun, and C. M. Jensen, J. Alloys Compd. **377**, 283 (2004).
[7] P. Wang and C. M. Jensen, J. Phys. Chem. B **108**, 15827 (2004).
[8] O. M. Løvvik, S. M. Opalka, H. W. Brinks, and B. C. Hauback, Phys. Rev. B **69**, 134117 (2004).
[9] P. Vajeeston, P. Ravindran, R. Vidya, H. Fjellvåg, and A. Kjekshus, Appl. Phys. Lett. **82**, 14 2257 (2003).
[10] P. Vajeeston, P. Ravindran, R. Vidya, H. Fjellvåg, and A. Kjekshus, Phys. Rev. B **68**, 212101 (2003).
[11] P. Ravindran, P. Vajeeston, H. Fjellvåg, and A. Kjekshus, Comput. Mater. Sci. **30**, 349 (2004).
[12] P. Vajeeston, P. Ravindran, A. Kjekshus, and H. Fjellvåg, Phys. Rev. B **69**, 020104(R) (2004).
[13] B. C. Hauback, H. W. Brinks, and H. Fjellvåg, J. Alloys Compd. **346**, 184 (2002).
[14] B. M. Bulychev, V. N. Verbetskii, and K. N. Semenenko, Russ. J. Inorg. Chem. **22**, 1611 (1977).
[15] K. Wakamori, A. Sawaoka, S. M. Filipek, and B. Baranowski, J. Less-Common Met. **88**, 217 (1982).
[16] Solid state chemistry, edited by R. Metselaar, H. J. M. Heijligers, and J. Schoonman, 1982 Proceedings of the Second European Conference, Veldhoven, The Netherlands, 7–9 June 1982, Studies in Organic Chemistry, Vol. 3; J. P. Bastide, B. M. Bonnetot, J. M. Letoffe, and P. Claudy, Structural Chemistry of some complex hydrides of alkaline metals, p. 785.
[17] J.-P. Bastide, J.-C. Bureau, J.-M. Letoffe, and P. Claudy, Mater. Res. Bull. **22**, 185 (1987).
[18] S. N. Konovalov, B. M. Bulychev, and V. K. Genchel, Russ. J. Inorg. Chem. **35**, 327 (1990).
[19] A. V. Talyzin and B. Sundqvist, Phys. Rev. B **70**, 180101(R) (2004).
[20] ISIS Annual Report, ISSN 1358-6254, 61 (1996).
[21] J. M. Besson, R. J. Nelmes, G. Hamel, J. S. Loveday, G. Weill, and S. Hull, Physica B **180–181**, 907 (1992).
[22] W. G. Marshall and D. Francis, J. Appl. Crystallogr. **35**, 122 (2002).
[23] A. C. Larson and R. B. Von Dreele, General Structure Analysis System (GSAS), Los Alamos National Laboratory Report LAUR 86-748, 2004.
[24] B. A. Hunter, Commission on Powder Diffraction Newsletter **20**, 21 (1998), http://www.iucr.org/iucr-top/comm/cpd/Newsletters/no20summer1998/art15/art15.htm
[25] C. S. Smith and K. O. McLean, J. Phys. Chem. Solids **34**, 1143 (1973).
[26] A. K. Tyagi, S. N. Achary, C. Karunakaran, and S. N. Vaidya, J. Mater. Sci. Lett. **19**, 1305 (2000).
[27] N. Herron, D. L. Thorn, R. L. Harlow, G. A. Jones, J. B. Parise, J. A. Fernandez-Baca, and T. Vogt, Chem. Mater. **7**, 75 (1995).
[28] J. M. Besson, G. Weill, G. Hamel, R. J. Nelmes, J. S. Loveday, and S. Hull, Phys. Rev. B **45**, 2613 (1992).
[29] U. Ruschewitz and R. Poettgen, Z. Anorg. Allg. Chem. **625**, 1599 (1999).
[30] T. W. D. Farley, W. Hayes, S. Hull, M. T. Hutchings, and M. Vrtis, J. Phys.: Condens. Matter **3**, 4761 (1991).
[31] N. Herron and W. E. Farneth, Adv. Mater. (Weinheim, Ger.) **8**, 959 (1996).
[32] A. Boultif and D. Louer, J. Appl. Crystallogr. **37**, 724 (2004).
[33] Accuracy in powder diffraction, edited by S. Block and C. R. Hubbard, NBS Spec. Publ. Vol. 567, 1980; R. Shirley, Data accuracy for powder indexing, 361.
[34] A. Le Bail, H. Duroy, and J. L. Fourquet, Mater. Res. Bull. **23**, 447 (1988).
[35] V. Favre-Nicolin and R. Cerny, J. Appl. Crystallogr. **35**, 734 (2002). Free Objects For Crystallography (FOX). Open source 2-theta version publicly available at http://objcryst.sourceforge.net. TOF version currently unavailable.
[36] D. Blanchard, H. W. Brinks, B. C. Hauback, and P. Norby, Mater. Sci. Eng., B **108**, 54 (2004).
[37] *Transition Metal Hydrides*, edited by R. Bau, Proceedings of the 2nd Joint Conference on Chemical Ins. Canada and Am. Chem. Soc, Montreal, Canada, May 1977, American Chemical Society, Washington, DC; A. C. Switendick, Electronic structure of transition metal hydrides, 264.
[38] J. J. Vajo, S. L. Skeith, and F. Mertens, J. Phys. Chem. B **109**, 3719 (2005).
[39] A. Zuttel, P. Wenger, P. Sudan, P. Mauron, and S. Orimo, Mater. Sci. Eng., B **108**, 9 (2004).